BIOCHEMISTRY
including biophysical chemistry & molecular biology

Article

pubs.acs.org/biochemistry

Effects of Proton Motive Force on the Structure and Dynamics of Bovine Cytochrome *c* Oxidase in Phospholipid Vesicles

Takashi Nomura,[†] Sachiko Yanagisawa,[†] Kyoko Shinzawa-Itoh,[‡] Shinya Yoshikawa,[‡] and Takashi Ogura*[,†,§]

[†]Laboratory of Spectroscopy, Graduate School of Life Science, University of Hyogo, RSC-UH Leading Program Center, Koto 1-1-1, Sayo-cho, Sayo-gun, Hyogo 679-5148, Japan

[‡]Laboratory of Protein Crystallization, Picobiology Institute, Graduate School of Life Science, University of Hyogo, Koto 3-1-1, Kamigori-cho, Ako-gun 678-1205, Japan

[§]Laboratory of Vibrational Spectroscopy, Picobiology Institute, Graduate School of Life Science, University of Hyogo, RSC-UH Leading Program Center, Koto 1-1-1, Sayo-cho, Sayo-gun 679-5148, Japan

Supporting Information

ABSTRACT: A conventional method for reconstituting cytochrome *c* oxidase (CcO) into phospholipid vesicles (COV) has been modified to permit resonance Raman (RR) analysis in the presence and absence of proton motive force ($\Delta\mu_H^+$). The COV has an average diameter of 20 nm and contains one CcO molecule within a unified orientation with Cu_A located outside the COV. The process of generation of $\Delta\mu_H^+$ across the membrane was monitored spectrophotometrically with rhodamine123 dye. The COV exhibits a respiratory control ratio (RCR) value of >30 and is tolerant to RR measurements with 10 mW laser illumination for 60 min at 441.6 nm. Structural perturbations at the heme sites caused by incorporation into vesicles were clarified by spectral comparisons between solubilized CcO and COV. Absorption spectroscopy revealed that the rate of electron transfer from cytochrome *c* to O_2 is reduced significantly more in the presence of $\Delta\mu_H^+$ than in its absence. RR spectroscopic measurements indicate that CcO in COV in the "respiratory-controlled" state adopts a mixed-valence state (heme a^{2+} and heme a_3^{3+}). This study establishes a supramolecular model system for experimentally examining the energy conversion protein machinery in the presence of $\Delta\mu_H^+$.

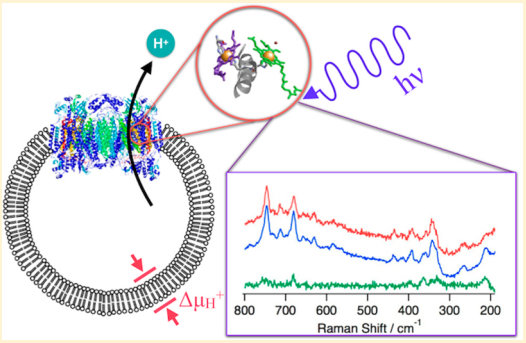

Since the proposal of the "chemiosmotic hypothesis" relating to the mitochondrial oxidative phosphorylation mechanism,[1] the structures and functions of the constituent membrane proteins have been a significant biochemical and biophysical concern for the past half-century. It has been established that four protons are pumped across the mitochondrial membrane when one O_2 molecule is reduced to H_2O by cytochrome *c* oxidase (CcO) in mitochondria (1:1 H^+:e^-).[2] The electron transfer rate in the respiration system is regulated by the proton motive force ($\Delta\mu_H^+$), which is defined as the sum of the electric potential ($\Delta\psi$) and the difference in pH across the membrane (ΔpH).[3] The coupling mechanism between electron and proton transfers mediated by CcO remains to be clarified. An "acceptor control" mechanism was identified in which the addition of ADP, an acceptor of P_i, increases the rate of electron transfer from NADH to O_2 via cytochrome *c* (cyt *c*),[4−7] while the reverse electron transfer from reduced cyt *c* (cyt c^{2+}) to NAD^+ occurs upon addition of ATP.[8] The electron transfer rate at the CcO site, on the other hand, depends on the relative concentrations of reduced and oxidized cyt *c*.[9] Therefore, the reactivity of CcO with O_2 must be regulated in a complex manner by $\Delta\mu_H^+$ as well as the concentrations of substrates.

The oxygen reduction mechanism has been extensively studied by resonance Raman (RR) spectroscopy[10−12] for solubilized CcO but has been studied to a much lesser extent for membrane-bound CcO.[13,14] An appropriate model system is needed to investigate the dependence of the structure and reactivity of CcO on $\Delta\mu_H^+$ and concentrations of substrates. Model liposomes have been constructed to examine the coupling between proton and electron transfer by CcO and to determine the H^+:e^- ratio[15−19] but have not been investigated by vibrational spectroscopy. The objective of this study was to prepare a supramolecular model system applicable to vibrational spectroscopic analyses based on CcO reconstituted into phospholipid vesicles (COV) for simulating the state of CcO in the mitochondrial membrane.

Preparations of mitochondria and model liposomes are characterized by what is known as the "respiratory control ratio" (RCR).[20] This parameter is defined as the ratio of the rate of electron transfer from cyt c^{2+} to O_2 in the absence of

Received: May 24, 2014
Revised: September 8, 2014
Published: September 17, 2014

dx.doi.org/10.1021/bi501022j | *Biochemistry* 2014, 53, 6382−6391

$\Delta\mu_H^+$ to that in the presence of $\Delta\mu_H^+$. It is presumed that the model COV exhibits a high RCR value and that $\Delta\mu_H^+$ is monitored concomitantly with a suitable dye. The RCR and $\Delta\mu_H^+$ values should be maintained for at least 10 min to measure the properties of CcO. To obtain RR spectra for determining the structural details of the heme of CcO, the COV should be tolerable to laser illumination for a certain period of time. We have observed in this study that the laser illumination used for the RR measurements produced the effect of significantly decreasing RCR values for COV prepared using the previously reported cholate dialysis method.[6] Furthermore, the orientation of the CcO molecule in COV should ideally be100% right-side out. In this study, we succeeded in providing a suitable supramolecular system that satisfies the prerequisites mentioned above for examining the structure and dynamics of CcO in COV.

MATERIALS AND METHODS

Materials. CcO was purified from bovine heart according to a previously published method.[21] The concentration of CcO was determined spectrophotometrically using an extinction coefficient of 46.6 mM^{-1} cm^{-1} for $\Delta A = A_{605} - A_{630}$ in the reduced state.[22] L-α-Phosphatidylcholine (PC) (chicken egg), L-α-phosphatidylethanolamine (PE) (bovine heart), and cardiolipin disodium salt (CL) (bovine heart) of the highest available grade were purchased from Avanti Polar Lipids, Inc. *N*-β-Decyl maltopyranoside was obtained from Anatrace. Cytochrome *c* was purchased from Nacalai Tesque. Calbiosorb adsorbent was purchased from Calbiochem. Other chemicals were of the highest grade commercially available and used without further purification.

Preparation of COV. Chloroform solutions of three different phospholipids (20 mg of PC, 3.2 mg of PE, and 3.2 mg of CL), the relative proportions of which are close to those in bovine heart mitochondria, were mixed (total volume of 1.04 mL) in a recovery flask (100 mL) and dried for 1.5 h to form a thin film. The film was dissolved in 3 mL of 100 mM HEPES-Na buffer (pH 7.4) supplemented with 25 mM cholate and then filtered with a 0.2 μm membrane filter (cellulose acetate, Advantec). CcO was added to the filtrate to a final concentration of 1 μM, and after being stirred for 5 min, the solution was subjected to the following four-step dialysis procedure: dialysis 1, against 300 mL of 100 mM HEPES-Na, pH 7.4 buffer for 4 h; dialysis 2, against 600 mL of 10 mM HEPES-Na, pH 7.4 buffer containing 27 mM KCl and 73 mM sucrose for 4 h; dialysis 3, against 600 mL of 1 mM HEPES-Na, pH 7.4 buffer containing 30 mM KCl and 80 mM sucrose for 12 h; and dialysis 4, against 600 mL of 2.5 mM HEPES-Na, pH 7.4 buffer containing 250 mM sucrose and 22.5 mM K_2SO_4 for 4 h. After dialysis, the solution was purified using an anion exchange column [Fractogel EMD DEAE (M), Merck Millipore] with a 10 mm diameter column and a 4 mL bed volume, pre-equilibrated with 2.5 mM HEPES-Na, pH 7.4 buffer containing 250 mM sucrose and 22.5 mM K_2SO_4. The bound sample was washed with 8 mL of 5 mM HEPES-Na, pH 7.4 buffer containing 200 mM sucrose and 45 mM K_2SO_4 and eluted with 8 mL of 20 mM HEPES-Na, pH 7.4 buffer containing 150 mM K_2SO_4. This column chromatography was effective for the removal of extra phospholipids and for increasing the degree of uniformity of the orientation of CcO in COV from 90 to 98% (with regard to the method of determination of the orientation of CcO in COV, as described below). Finally, the sample was dialyzed for 10 min three times against the buffer used for measurements (600 mL of 2.5 mM HEPES-Na, pH 7.4 buffer containing 49 mM KCl, 16 mM sucrose, and 80 mM choline chloride) and concentrated with a membrane filter (Amicon Ultra Centrifugal Device, 100 kDa, Millipore), followed by centrifugation at 900*g* for 60 min to a COV concentration of 1.5−2.1 μM (in terms of CcO). All reconstitution procedures were performed at 4 °C.

The sample obtained as described above is defined as sample 1. Because it was not sufficiently tolerable to laser illumination as described below, 3 g of detergent adsorbent (Calbiosorb) was added to the dialysis 4 buffer while all the other procedures were unaltered. This sample is defined as sample 2. To further improve the tolerance against prolonged laser illumination, an additional 2 h dialysis against 600 mL of 1 mM HEPES-Na, pH 7.4 buffer containing 30 mM KCl and 48 mM sucrose was adopted between dialysis 2 and dialysis 3, while all other procedures were unaltered. This sample is defined as sample 3.

The orientation of CcO in COV was determined by examining the level of reduction of COV using cyt c^{2+} and $Na_2S_2O_4$ as reductants. When COV was reduced by ascorbate in the presence of cyt *c* under anaerobic conditions, only CcO with the correct orientation (with Cu_A located outside the membrane, as in mitochondria) was reduced. On the other hand, all of the CcO present is reduced by addition of $Na_2S_2O_4$ irrespective of its orientation. The level of reduction monitored by the absorbance ratio at 442 nm indicates that the proportion of COV with the correct orientation is 98%.

The concentration of cyt c^{2+} was determined by the absorbance at 550 nm. The sample used for electron microscopy (EM) was prepared by negative staining (3 μL of 13 nM COV was treated with uranyl acetate) and applied to a Cu grid. EM images of COV were observed using a JEM-2010 electron microscope (Nihon Denshi).

Measurement of the Respiratory Control Ratio (RCR). For measurements of RCR, the time-dependent decrease in absorption of cyt c^{2+} at 550 nm was recorded on a spectrophotometer (V-630, Jasco), as illustrated in Figure S1 of the Supporting Information, where the slope of the trace represents the rate of electron transfer. The RCR value was determined by dividing the rate measured in the absence of $\Delta\mu_H^+$ (V_2) by the rate measured in its presence (V_1). COV was added to a 2 mL volume of the reaction mixture consisting of 20 μM cyt c^{2+}, 2.5 mM HEPES-Na (pH 7.4), 49 mM KCl, 16 mM sucrose, and 80 mM choline chloride to a final concentration of 2 nM (in terms of CcO) to start the reaction, and its rate (V_1) corresponds to the value in the presence of $\Delta\mu_H^+$. Then, ionophores, including valinomycin and carbonyl cyanide-*p*-trifluoromethoxyphenylhydrazone (FCCP), were added to the reaction mixture to final concentrations of 15 and 10 μM, respectively, to completely eliminate $\Delta\mu_H^+$. Again, the rate (V_2) was determined in the same way to provide the value in the absence of $\Delta\mu_H^+$. The temperature was maintained at 20 °C.

Measurement of Raman and Absorption Spectra. To measure absorption and RR spectra simultaneously, a quartz rectangular cell with five transparent walls (inner cross section of 4.5 mm × 4.5 mm, height of 50 mm) was used, and the two different spectra were measured in orientations perpendicular to each other (see Figure S2 of the Supporting Information). To regulate the gas phase in the cell, the upper part of the quartz cell was connected to a glass tube, which allows hermetic sealing of the cell with a rubber septum. To maintain the humidity of the gas phase in the cell, N_2 gas that was

dx.doi.org/10.1021/bi501022j | *Biochemistry* 2014, 53, 6382−6391

prebubbled through temperature-controlled water was purged during the measurements, and the sample solution was always stirred with a Teflon-coated magnetic bar. The cell was placed in a water-jacketed holder, and thermostatic water was circulated to maintain the sample temperature at 20 °C.

Absorption spectra were measured between 350 and 700 nm at 5 s intervals using a multichannel CCD array detector (USB4000, Ocean Optics) and a tungsten lamp as a light source while the samples were being stirred. Quartz optical fibers with a core diameter of 400 μm were used to deliver light for absorption measurements. The measurement points of RR and absorption spectra were made as close as possible.

A 135° backscattering geometry was adopted for RR measurements. The laser beam was focused on the cell using a cylindrical lens (f = 100 mm) to define a line illumination area (width of 0.1 mm, height of 2 mm). The 441.6 nm line from a He/Cd laser (model IK5651R-G, Kimmon Koha) was used to excite RR scattering. The scattered light was detected with a liquid nitrogen-cooled CCD detector (CCD-1024×256-OPEN-1LS, Horiba Jobin Yvon) attached to a 1 m focal length polychromator (MC-100DG, Ritsu Oyo Kogaku) with a holographic grating of 1200 grooves/mm blazed at 500 nm. A holographic edge filter for 441.6 nm was used to reject Rayleigh scattering (LP02-442RE, Semrock). The spectral slit width was 6 cm^{-1}. The Raman shift was calibrated with indene as the frequency standard, and the wavenumber accuracy was ±1 cm^{-1} for well-resolved intense bands. The linear baseline was subtracted from the RR spectra observed for COV to eliminate the broad fluorescence background. To measure the RR spectra of static COV and solubilized CcO in the reduced state, $Na_2S_2O_4$ was added to a final concentration of 1 mM in the hermetically sealed cell under a N_2 atmosphere.

Measurements of Membrane Potential Using Rhodamine123 Dye. The membrane potential ($\Delta\Psi$) generated in COV was monitored by using rhodamine123 (Rh), which is a common reagent for examining mitochondria in the cell.[23] However, we found that it is important to use Rh under specific proper conditions because Rh can reflect the membrane potential of the phospholipid vesicle only when the outside is positive and the inside is negative in the neutral-pH region outside the membrane. Moreover, because Rh is also sensitive to absolute pH, it is important to discriminate between changes due to membrane potential and a simple pH change.

The absorption spectrum of isolated Rh shown in Figure S3a of the Supporting Information exhibits a spectral change when Rh is incorporated into the phospholipid vesicles used in this experiment, as shown in Figure S3b of the Supporting Information. For the vesicle prepared at pH 9.25 without ionophores, the absorbance at 524 nm (not the absorption peak, as will be discussed below) appreciably increases and then slowly decreases when HCl is added to the solution (Figure S4a of the Supporting Information). This is in contrast to the larger increase in absorbance observed at 524 nm with no later change in the presence of an ionophore (Figure S4b of the Supporting Information). This change reflects a simple pH change. The limited instantaneous increase in absorbance indicates the magnitude of the membrane potential generated. This absorbance intensity decays slowly because of proton leakage. When the difference in pH (ΔpH) between the outside and the inside is greater, the change in absorbance is greater as shown in panels a′ and b′ of Figure S4 of the Supporting Information. When the intensities of instantaneous absorbance increases are plotted against ΔpH, a linear relationship is evident as demonstrated in Figure S5 of the Supporting Information. Thus, it has been established that the absorbance of Rh at a certain wavelength indicates the membrane potential under these experimental conditions ($positive_{out}/negative_{in}$ in the neutral-pH region). However, it is noted that Rh does not indicate the membrane potential for the reverse direction [$negative_{out}/positive_{in}$ (not shown)].

In the COV measurements, cyt c is used as an electron carrier. cyt c has an absorption in this wavelength region as shown in Figure S6 of the Supporting Information, and it changes in different redox states. Therefore, spectral changes of cyt c overlap with the spectral change of Rh. To specifically observe the change of Rh, we monitored the change in absorbance of Rh at 524 nm, which is the isosbestic point of spectra of cyt c^{2+} and cyt c^{3+}. The absorbance of Rh at 524 nm is not influenced by the redox change of cyt c even in the presence of cyt c.

Preparation of Reduced COV in the Presence and Absence of $\Delta\mu_H^+$. The $\Delta\mu_H^+$ across the COV membrane was generated by proton pumping by COV itself. Concentrations of COV and Rh in the reaction buffer [2.5 mM HEPES-Na (pH 7.4), 49 mM KCl, 16 mM sucrose, and 80 mM choline chloride] were 2 μM (in terms of CcO) and 10 μM, respectively. Addition of cyt c (final concentration of 30 μM) to the 0.2 mL of the COV solution in the presence of ascorbate (final concentration of 25 mM) initiated the reduction of O_2 and concomitant proton pumping to generate $\Delta\mu_H^+$. These concentrations were determined by trial and error so that reduction of CcO is complete within 5 s. After CcO reached the fully reduced state, the gas phase of the cell was replaced with pure N_2 to protect CcO from further reaction with O_2. RR spectra were recorded at 1 min intervals. In separate experiments, the solution was preincubated with 15 μM valinomycin and 10 μM FCCP to eliminate $\Delta\mu_H^+$, and the same measurements were performed. It was confirmed that both valinomycin and FCCP do not produce measurable Raman bands at this concentration.

Preparation of Mixed-Valence and CN^--Bound ($a^{2+}a_3^{3+}$-CN^-) COV. To obtain COV-containing CN-bound fully reduced CcO ($a^{2+}a_3^{2+}$-CN^-), 100 mM KCN in 100 mM NaOH was added to the COV containing fully reduced CcO to a final concentration of 2 mM and the pH was immediately adjusted to 7.4 by addition of an appropriate amount of HCl. To produce the mixed-valence state, the COV solution was exposed to air for a short time. The formation of mixed-valence CN^--bound ($a^{2+}a_3^{3+}$-CN^-) COV was confirmed by absorption spectroscopy.[24]

RESULTS

Examples of the observed time-dependent absorption change of cyt c^{2+} in the presence and absence of $\Delta\mu_H^+$ are shown in Figure S1 of the Supporting Information. The ratio of V_1 to V_2 provides the RCR value. Table 1 summarizes the RCR values of samples 1−3 after laser irradiation at 441.6 nm with several different laser powers ranging from 0 to 10 mW for 60 min. All values are an average of not fewer than three measurements, and the number after the ± symbol denotes the standard deviation.

Figure 1 is a plot of the RCR values of Table 1 versus laser power. The red triangles denote the points obtained for sample 1. The RCR value at 0 mW (16.5) was relatively high compared with the reported values,[16,17] but it declined to 8.7 after illumination with the 10 mW laser. We added 3 g of detergent

dx.doi.org/10.1021/bi501022j | Biochemistry 2014, 53, 6382−6391

Table 1. RCR Values for COV Samples Illuminated by Laser Light at 441.6 nm[a]

laser power (mW)	RCR		
	sample 1	sample 2	sample 3
0	16.5 ± 4.1 (n = 3)	18.5 ± 4.3 (n = 3)	35.8 ± 4.8 (n = 13)
2	–	–	26.3 ± 1.7 (n = 3)
3	–	–	26.7 ± 2.1 (n = 3)
4	–	–	25.6 ± 2.8 (n = 3)
5	14.0 ± 2.2 (n = 3)	16.7 ± 0.5 (n = 3)	23.7 ± 2.0 (n = 4)
10	8.7 ± 1.7 (n = 3)	16.0 ± 1.4 (n = 3)	22.4 ± 0.5 (n = 3)

[a]Values are averages of n times independent experiments in parentheses. Values after the ± symbol denote the standard deviation.

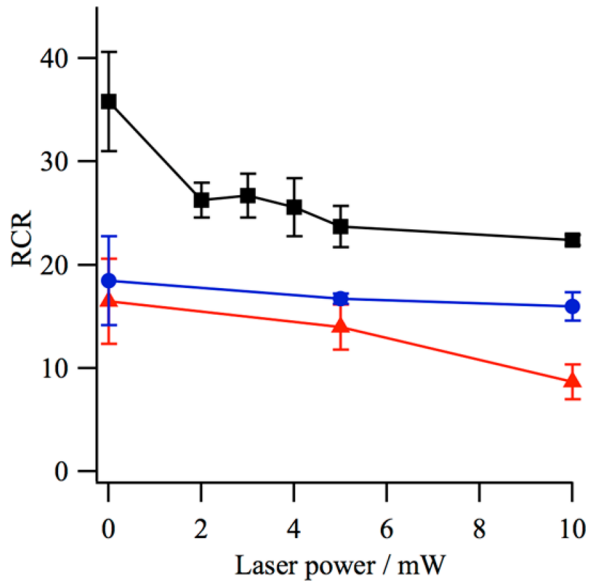

Figure 1. Plot of RCR vs laser power. The red triangles, blue circles, and black squares are for samples 1–3 of COV, respectively. Illumination with laser light at 441.6 nm was provided for 60 min under the same conditions used for RR measurements. Data are from Table 1, and the value of each point is the average of n times independent experiments shown in parentheses in Table 1. Error bars are based on the standard deviation. Solid lines are provided for the sake of clarity.

adsorbent (Calbiosorb) to the dialysis buffer and measured three data points [sample 2 (blue circles in Figure 1)]. In this case, although the change in the basal RCR value at 0 mW was insignificant (18.5 vs 16.5), the decrease after 10 mW illumination was found to be effectively protected (16.0 vs 8.7). Incorporation of an additional 2 h dialysis procedure [sample 3 (black squares in Figure 1)] significantly improved the RCR value (35.8). There was an extreme decline of the RCR value after illumination at 2 mW to 26.3. However, the change in the RCR value observed after illumination with a laser power increased to 10 mW was found to be insignificant. The RCR value of sample 3 after 10 mW laser illumination is significantly higher than that of sample 2. This indicates that sample 3 is tolerant of 10 mW laser illumination. On the other hand, sample 2 shows almost no dependence of RCR on power. These results indicate that samples 2 and 3 behave qualitatively in a different manner when they are subjected to laser illumination. This could be dependent on the manner of perturbation of the COV. However, the origin of the difference is an open question. The values listed in Table 1 are much higher than those of other functional vesicles.[15−19] Hereafter, all the COV data presented in this article were obtained from measurements of sample 3 with a laser power of 10 mW, because sample 3 exhibited the highest RCR value.

Figure 2 shows the absorption spectra of COV (black) and "solubilized" CcO (red) in the reduced state. The apparent

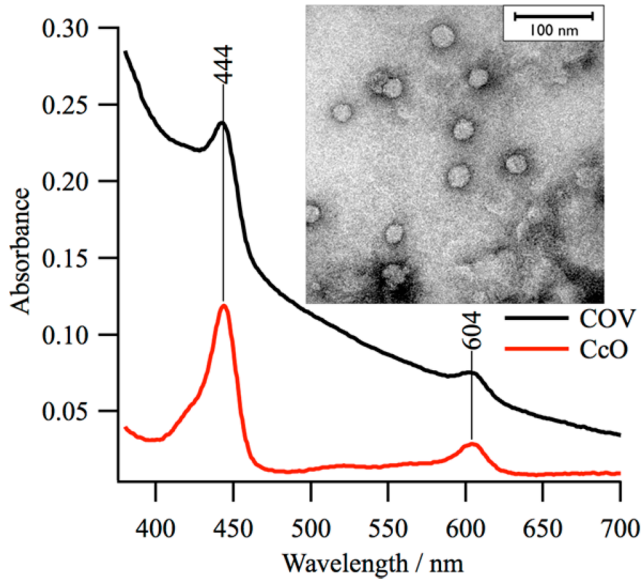

Figure 2. Absorption spectra of COV (black) and solubilized CcO (red). The concentrations of COV and CcO are 2.0 μM in each case. The inset shows the electron microscope image of COV.

absorbance of COV increases at shorter wavelengths because of light scattering. However, the heme-based absorption bands evident at 444 and 604 nm are essentially the same as those of solubilized CcO. The inset shows an electron microscopy image of a COV suspension. We note that the COV size is homogeneous and has an average diameter of 20 nm.

Figure 3A shows the absorbance changes at three selected wavelengths caused by addition of reductant or N_2 gas and indicates reduction levels of cyt c (550 nm) and CcO (443 nm) and the level of $\Delta\mu_H^+$ (524 nm). The solid lines are for COV in the presence of $\Delta\mu_H^+$, and the broken lines are for COV in the absence of $\Delta\mu_H^+$ (in the presence of ionophores). The T_m (m = 1–5) notations in Figure 3A show the time of each addition. At T_1, ascorbate is added aerobically as an electron donor to a final concentration of 25 mM. At T_2, cyt c^{3+} was added to a final concentration of 30 μM and produces changes in absorbance at 550 and 443 nm. At this stage, all of the components of the electron transfer system have been added and the electron transfer from ascorbate to O_2 is initiated. The 524 nm trace exhibits an increase due to the absorption of cyt c, and 524 nm is the isosbestic point between cyt c^{3+} and cyt c^{2+} as mentioned above.

Because O_2 is present in the gas phase and a sufficient amount of ascorbate is present, a steady state should be generated in the COV solution at T_2. The reduction level of cyt c as monitored at 550 nm becomes significantly higher in the absence of ionophores (solid line) than in their presence (broken line). This is ascribed to a slower rate of electron transfer from cyt c^{2+} to COV in the presence of $\Delta\mu_H^+$. In its

dx.doi.org/10.1021/bi501022j | Biochemistry 2014, 53, 6382–6391

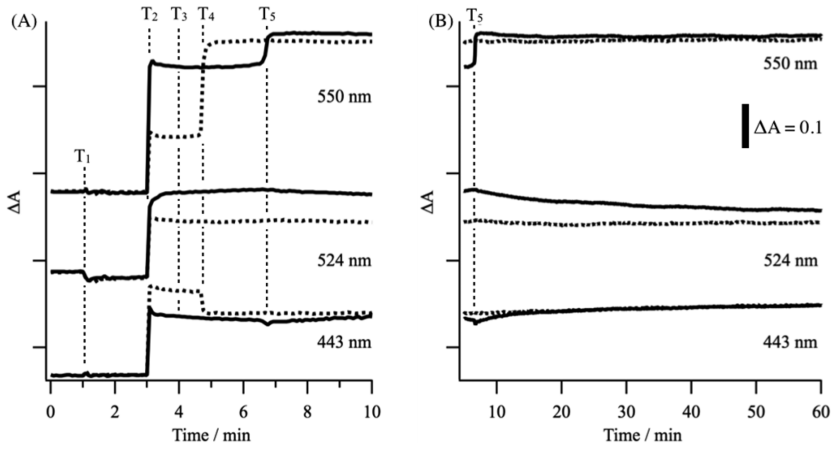

Figure 3. Time-dependent absorbance change at 550, 524, and 443 nm. The solid line and the broken line indicate the values obtained in the absence and presence of ionophores, respectively: (A) for 0−10 min and (B) for 5−60 min. T_1 (1 min): addition of sodium ascorbate (25 mM). T_2 (3 min): addition of cyt *c* (30 μM). T_3 (4 min): introduction of N_2 gas into the gas phase of the cell. T_4 (4.8 min): full reduction of cyt *c* attained in the absence of $\Delta\mu_H^+$. T_5 (6.8 min): full reduction of cyt *c* attained in the presence of $\Delta\mu_H^+$. Absorption spectra were recorded without laser illumination to prevent decomposition of rhodamine123. The concentration of COV was 1.8 μM. The absorbance change due to the volume change has been compensated. The absorbance scale (ΔA) is common to panels A and B and is shown only in panel B.

absence, however, the rate of electron transfer to COV is higher, and as a result, the equilibrium concentration of cyt c^{2+} decreases. At 443 nm, the absorbance is higher in the presence of the ionophore (broken line), which means that CcO is reduced to a greater extent in the absence of $\Delta\mu_H^+$. It is expected from the present path length of the cell (4.5 mm) and 30 μM cyt *c* that the absorbance at 550 nm increases by 0.25 and that the absorbance at 443 nm decreases by 0.11 when all of the added cyt c^{3+} is converted to cyt c^{2+}, and in addition, the absorbance of CcO at 443 nm is 0.05 when CcO is completely reduced. The $\Delta\mu_H^+$ generated in the absence of ionophores causes the difference between the solid and broken lines of the 524 nm traces. The absorbance difference of Rh at 524 nm is ΔA = 0.048, which corresponds to ΔpH = 8 on the basis of Figure S5 of the Supporting Information and is an extraordinarily large value. Here, the absorbance difference of 0.048 is obtained relative to the value at 60 min in the absence of ionophores instead of relative to the value at T_5 in the presence of ionophores. The volume inside the vesicle (diameter of 20 nm) is calculated to be extremely small (4.2×10^{-21} L), and therefore, the number of protons inside COV based on pH definition is extremely small. However, protons are actually pumped out. Therefore, protons are likely to be supplied from buffer and protein systems.

At T_3, the inside gas phase of the cell (air) is replaced with pure N_2. After some time, the remaining O_2 is exhausted and the reaction stops. At this stage (at T_4), full reduction of cyt *c* and CcO is attained in the stationary state in the presence of the ionophore. When cyt c^{3+} is converted to cyt c^{2+}, the absorbance at 443 nm of cyt *c* is reduced by 0.1 absorbance unit (see Figure S6 of the Supporting Information) but the absorbance of CcO increases by 0.05, and as a result, a reduction in absorbance of 0.05 is observed for the broken line of the 443 nm trace. The 0.22 increase in absorbance observed at 550 nm is consistent with this interpretation.

In the presence of $\Delta\mu_H^+$, however, the complete reduction of cyt *c* is attained much later at T_5 as seen for the solid line of the 550 nm trace. The increase in the absorbance of cyt *c* at 550 nm by 0.1 is accompanied by a reduction in the absorbance intensity at 443 nm of 0.05. Reduced CcO contributes to the absorbance at 443 nm (absorption maximum of reduced CcO), and the actual absorbance change at 443 nm is 0.025, indicating that CcO is not fully reduced at T_5. We note that the level of reduction of cyt *c* is higher in the presence of $\Delta\mu_H^+$ than in the absence of $\Delta\mu_H^+$ at T_5. The 524 nm trace indicates the generation of $\Delta\mu_H^+$ at T_2 in the absence of ionophores, while the magnitude of $\Delta\mu_H^+$ present is reflected by the difference between the solid and broken lines.

The 524 nm trace exhibits a two-phase decay profile, if analyzed numerically, with time constants of 5.0 ± 0.9 and 95 ± 54 min (n = 3) from T_5 as illustrated in Figure 3B. Here, the number indicated by "*n*" in parentheses denotes the number of independent experiments performed to calculate the average value and the standard deviation. The slower phase becomes significantly faster with laser illumination and therefore is ascribed to decomposition of Rh. Thus, the results indicate that the generated $\Delta\mu_H^+$ exhibits a decay with a time constant of 5.0 min. The solid 443 nm trace reveals that COV is not fully reduced at T_5. Instead, the fully reduced state is approached from T_5 through two phases with time constants of 3.0 ± 1.4 and 14 ± 11 min (n = 3), and their fractional amplitudes are 49 and 51%, respectively. Because the second phase can also be detected in the absence of $\Delta\mu_H^+$ (broken trace for 443 nm) for an unknown reason, we discuss only the first phase. The presence of the first phase (τ = 3.0 min) in the presence of $\Delta\mu_H^+$ is a notable difference compared with the abrupt reduction of COV in the absence of $\Delta\mu_H^+$ at T_4. The time constant of $\Delta\mu_H^+$ decay (5.0 ± 0.9 min) is comparable to that of reduction of COV (3 ± 1.4 min).

Figure 4 shows the absorption spectra of COV in the presence of $\Delta\mu_H^+$ at T_5 (red) and in its absence at 60 min (blue). The green trace shows their difference (blue minus red). The fractional population of reduced COV as estimated from the absorbance at 443 nm in the difference spectrum is 45 ± 4% (n = 4). This value is identical to the value obtained for the laser-illuminated sample. This indicates that the COV containing Rh is generally stable during the process of measuring the RR spectra.

We examined RR spectra to observe the structural effects of membranes on CcO molecules in COV. Figure 5 shows the RR spectra of reduced COV (A and A′) and solubilized CcO (B and B′), and their difference spectra (C = B − A, and C′ = B′ −

dx.doi.org/10.1021/bi501022j | *Biochemistry* 2014, 53, 6382−6391

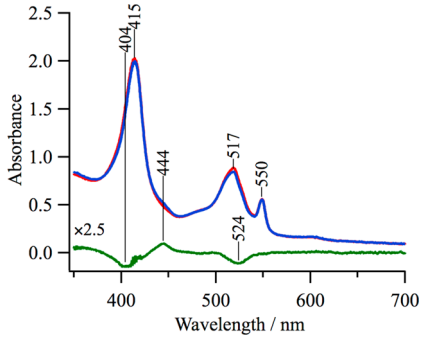

Figure 4. Absorption spectra of fully reduced COV in the presence (red) and absence of $\Delta\mu_H^+$ (blue). Red and blue spectra were recorded at T_5 and 60 min later. The accumulation time for each spectrum was 750 ms. The difference absorption spectrum (blue minus red) is colored green. The absorption maxima at 415 and 550 nm arise from reduced cyt *c*, and the absorption maximum at 517 nm originates from rhodamine123.

A′). It is noted that the quality of the RR spectrum of COV is equivalent to that of soluble CcO. The difference feature is more prominent in the low-frequency region (190−800 cm^{-1}) than in the high-frequency region (800−1700 cm^{-1}), indicating that structural perturbations influence the peripheral substituents of the heme macrocycle as a result of reconstitution of the enzyme into phospholipid vesicles.

Figure 6 shows RR spectra of COV in the (A) presence and (B) absence of $\Delta\mu_H^+$ and their difference (C = B − A). Spectra 6A and 6A′ were obtained for 5 and 1 min accumulations from T_5, respectively. The intensity of the band at 213 cm^{-1}, which arises from the Fe−N(His) stretching mode of reduced heme a_3,[25] is significantly higher in spectrum 6A than in spectrum 6A′. In addition, there are two bands at 364 and 357 cm^{-1} in spectrum 6A, but only one band at 357 cm^{-1} in spectrum 6A′. These bands are assigned to the γ_6 mode[26−28] (pyrrole tilting) of reduced heme a_3 and heme *a*, respectively. These RR spectral changes occur almost synchronously with a change in $\Delta\mu_H^+$, reflecting the electron transfer to heme a_3.

The band at 213 cm^{-1} in spectrum 6C indicates the decrease in the intensity of this mode in the presence of $\Delta\mu_H^+$, suggesting that heme a_3 is partially oxidized, because the oxidized heme a_3 does not yield the 213 cm^{-1} band. In fact, this spectrum is close to the reported spectrum of solubilized CcO in the mixed-valence state ($a^{2+}a_3^{3+}$).[24] ("*a*" and "a_3" represent Fe of heme *a* and heme a_3, respectively, and the superscript denotes the oxidation state of Fe.) To obtain further insights into COV in electron-rich and O_2-poor environments in the presence of $\Delta\mu_H^+$, we prepared a cyanide-bound mixed-valence version of COV ($a^{2+}a_3^{3+}$-CN^-) and compared its RR spectrum with that of fully reduced COV ($a^{2+}a_3^{2+}$), because there have been no reports of RR spectra of the former species of COV.

Figure 7 shows the RR spectra of fully reduced ($a^{2+}a_3^{2+}$) (A) and mixed-valence and CN^--bound COV ($a^{2+}a_3^{3+}$-CN^-) (B) and a difference spectrum (C = A − B). The inset shows the absorption spectra of the species corresponding to each of the RR spectra. The excitation wavelength of 441.6 nm is very close to the absorption maximum at 443 nm of $a^{2+}a_3^{2+}$ but also close to the maxima of $a^{2+}a_3^{3+}$-CN^- at 443 nm (a^{2+}) and 425 nm (a_3^{3+}-CN^-). Therefore, excitation at 441.6 nm preferentially reveals the vibrational spectrum of CcO rather than the spectra of cyt *c* and Rh that are also present. We note that spectrum 6C is essentially identical to spectrum 7C except for the presence of the 276 cm^{-1} band in the latter. We ascribe the apparent absence of the 276 cm^{-1} band in spectrum 6C to the much

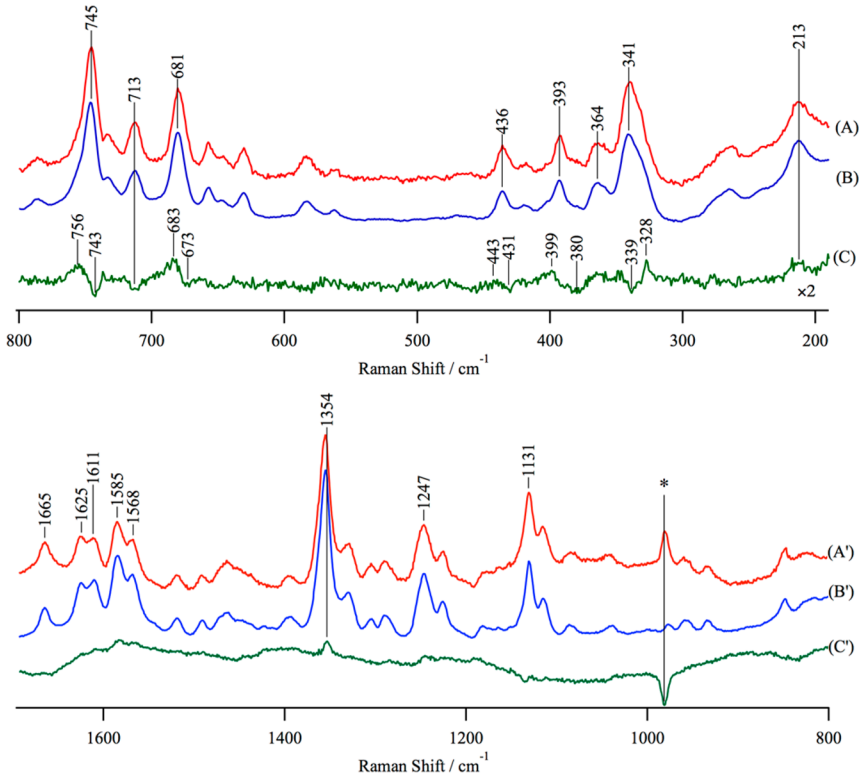

Figure 5. Resonance Raman spectra of (A and A′) reduced COV and (B and B′) reduced solubilized CcO and (C and C′) Raman difference spectra (C = B − A, and C′ = B′ − A′). The band marked with an asterisk is due to $(NH_4)_2SO_4$, which is present in the solubilized CcO solution.

dx.doi.org/10.1021/bi501022j | *Biochemistry* 2014, 53, 6382−6391

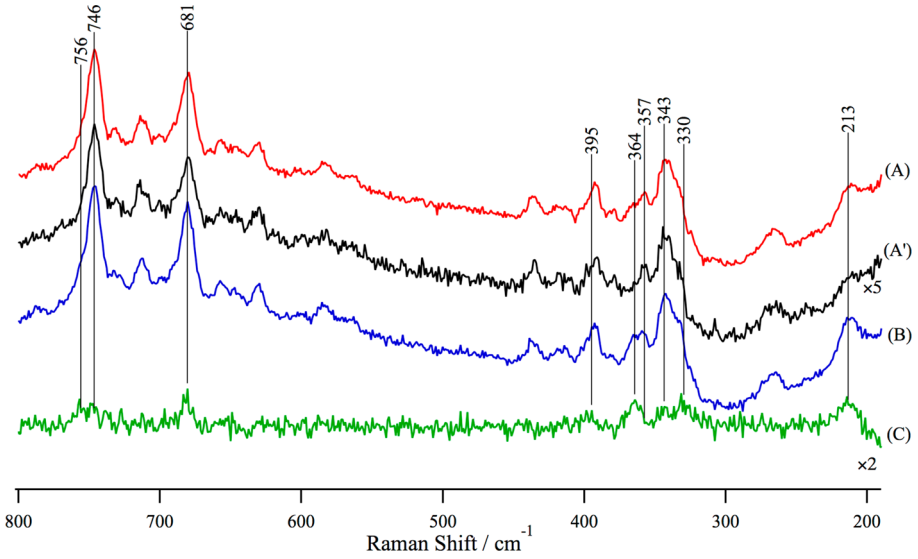

Figure 6. Resonance Raman spectra of fully reduced COV. (A) Accumulated for 5 min between T_5 and T_5 + 5 min. (A′) Accumulated for 1 min between T_5 and T_5 + 1 min. (B) Accumulated for 5 min between 60 and 65 min. (C) Difference spectrum (C = B − A). Spectra A, A′, and B were obtained from the sum of five accumulated spectra. RR spectra were recorded in a manner independent of absorption measurements shown in Figure 3, but the elapsed times from T_1 to T_5 are common between Figures 3 and 6. The concentration of COV was 1.7 μM.

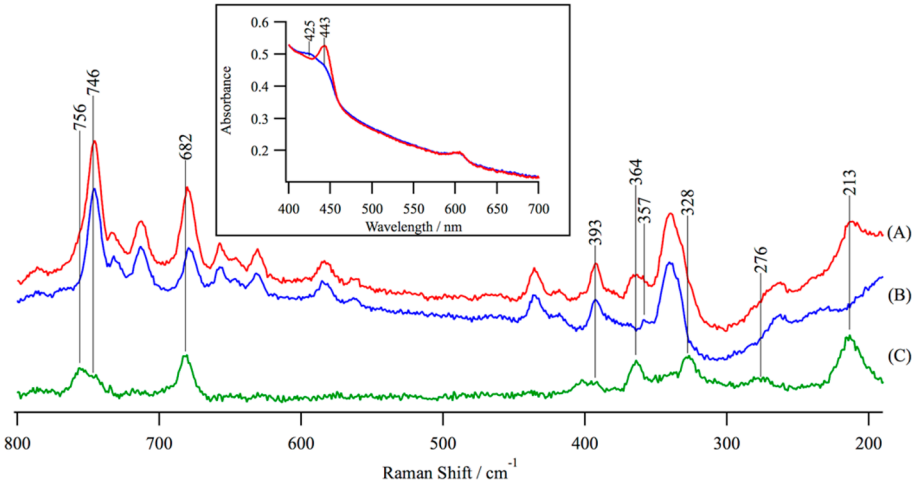

Figure 7. Resonance Raman spectra of (A) fully reduced COV ($a^{2+}a_3{}^{2+}$) and (B) mixed-valence and cyanide-bound COV ($a^{2+}a_3{}^{3+}$-CN^-). (C) Raman difference spectrum obtained by subtracting Spectrum B from Spectrum A. The concentration of COV is 1.7 μM. The inset shows absorption spectra of $a^{2+}a_3{}^{2+}$ (red) and $a^{2+}a_3{}^{3+}$-CN^- (blue).

lower signal-to-noise ratio. Therefore, the results indicate that COV placed in the electron-rich and O_2-poor environments adopts the $a^{2+}a_3{}^{3+}$ state in the presence of $\Delta\mu_H{}^+$.

DISCUSSION

Preparation of COV Suitable for RR Analysis. COV was initially used to study the mechanism of energy conversion in mitochondria by CcO[16] and then to determine the H^+:e^- ratio for the electron-driven proton pump.[15,17−19] The coordination structures of heme a_3 in the reaction intermediates of solubilized CcO have been extensively studied by RR spectroscopy,[10−12] and it was found that they are the same in the native mitochondria and solubilized enzyme.[14,29] Because the presence of the membrane system is required to study the effects of $\Delta\mu_H{}^+$ on the structure and dynamics of the hemes, usage of COV is desirable as the simplest supramolecular model of the respiration enzymes. Three-dimensional structures of CcO have been determined with high resolution (1.8 Å),[30] and it is known that an electron is passed to Cu_A from cyt c^{2+} on the outside and then transferred to heme a_3 through heme a.[2] CcO in the COV should behave in a manner similar to that of CcO in mitochondria as a model system. This means that COV is reduced by cyt c^{2+} and functional as a proton pump. This requirement is satisfied in our model, because the present COV is 98% right-side out. The diameter of COV as viewed by electron microscopy is approximately 20 nm, suggesting that a single CcO molecule is embedded in each COV.

The model COV should retain a high RCR value for a longer period, because otherwise the generated $\Delta\mu_H{}^+$ ceases to exist during Raman measurements. Sample 1 exhibits a decrease in RCR from 16.5 to 8.7 after laser illumination (Table 1 and Figure 1). Therefore, in this study, significant efforts were made to improve the method for preparing COV. We noted that addition of detergent adsorbent (Calbiosorb) to the dialysis medium of dialysis 4 improved the tolerance to laser illumination as demonstrated for sample 2. Incorporation of

dx.doi.org/10.1021/bi501022j | Biochemistry 2014, 53, 6382−6391

additional dialysis conditions between dialyses 2 and 3 significantly increased the RCR value to 35.8 before laser illumination and >22 after laser illumination. This means that removal of cholate is essential to obtain high RCR values, while the tolerance to laser illumination is different. However, the RCR value remains at 22 after laser illumination, and this is much higher than the value required for functional experiments.[15−19] Accordingly, in this study, we used sample 3 to record absorption and RR spectra.

Effect of $\Delta\mu_H^+$ on COV. The traces in Figure 3 demonstrate that $\Delta\mu_H^+$ monitored by absorbance at 524 nm clearly changes at the start of the reaction at T_2 and remains constant afterward. In addition, the stationary state concentrations of cyt c^{2+} under electron-rich and O_2-deficient conditions are different in the absence (T_4) and presence (T_5) of $\Delta\mu_H^+$. This difference arises from slight differences in the rate of electron transfer from cyt c^{2+} to COV. The absorption spectra shown in Figure 4 indicate that approximately 50% of COV is in the oxidized state at T_5 in the presence of $\Delta\mu_H^+$ under anaerobic conditions. The time constant for reduction of the remaining 50% of CcO is 3 min as determined by the 443 nm solid line in Figure 3B.

The RR spectrum that accumulated in the time window between T_5 and T_5 + 5 min clearly exhibits the $\nu_{Fe\text{-}His}$ mode (spectrum 6A), while the spectrum that accumulated in the time window between T_5 and T_5 + 1 min exhibits a significantly weaker $\nu_{Fe\text{-}His}$ mode (spectrum 6A′). These observations indicate that the intensity of the $\nu_{Fe\text{-}His}$ mode grows over the course of 5 min. This is consistent with the time constant (3 min) mentioned above. The intensity of the $\nu_{Fe\text{-}His}$ mode would reach zero if time is extrapolated to T_5. Thus, the $\nu_{Fe\text{-}His}$ mode can be used as a marker of reduced heme a_3.[25] The intensity of the RR band at 357 cm^{-1} is constant in spectra 6A, 6A′, and 6B, while the intensity of the band at 364 cm^{-1} is negligible in spectrum 6A′ but increases from spectrum 6A to spectrum 6B. The band at 364 cm^{-1} has been reported to arise from heme a_3 in the reduced and high-spin state like the $\nu_{Fe\text{-}His}$ mode. This band loses its intensity upon binding of CN^-.[25]

The band at 364 cm^{-1} is assigned to the pyrrole tilting mode of the porphyrin (γ_6)[26−28] of heme a_3^{2+}. The band at 357 cm^{-1} is assigned to the γ_6 mode of heme a^{2+}.[24] Therefore, these two bands at 364 and 357 cm^{-1} could be used as markers for the oxidation state of hemes a_3 and a, respectively. These results provide a strong indication that COV adopts the $a^{2+}a_3^{3+}$ oxidation state under "respiratory-controlled" conditions by lowering the rate of electron transfer from cyt c^{2+} to COV. This is consistent with the fact that the reduction level of cyt c is higher in the presence of $\Delta\mu_H^+$ than in its absence (the 550 nm trace in Figure 3 at T_5). In contrast, under the steady state turnover conditions with relatively high levels of ascorbate and O_2, intramolecular electron transfer from heme a to heme a_3 is the rate-limiting step.[31]

Structural Effects on Hemes of CcO Caused by Its Reconstitution into COV. The observation that there is no noticeable difference in Figure 5 between solubilized CcO and COV in the higher-frequency modes (800−1700 cm^{-1}) indicates that the heme macrocycle is not significantly affected by the reconstitution of CcO into COV. However, several RR bands of COV in the lower-frequency region (190−800 cm^{-1}) exhibit frequency shifts and/or intensity changes compared with "solubilized" CcO. The RR band at 436 cm^{-1} is assigned to the δ_{vinyl} (C_β−CH═CH_2 bending) mode of heme a^{2+}.[24,32] Reconstitution of CcO into COV causes a low-frequency shift of the band (443 cm^{-1}/431 cm^{-1} difference in spectrum 5C). This suggests that the steric effects of helix X (an α-helix) on the vinyl group of heme a in COV have been reduced.

The intensity of the $\nu_{Fe\text{-}His}$ stretching mode at 213 cm^{-1} decreases in COV without any frequency shift (Figure 5). The appearance of the $\nu_{Fe\text{-}His}$ mode indicates the presence of five-coordinate high-spin reduced heme a_3.[25] Because COV and CcO are both in the fully reduced state in Figure 5, the difference in intensity cannot be ascribed to contamination with the oxidized state. The change in intensity of the $\nu_{Fe\text{-}His}$ mode might be caused by a change in the tilt angle of the Fe−His bond with respect to the heme normal, the azimuthal angle of the His plane, or the out-of-plane displacement of Fe ion from heme.[33,34] Although we cannot conclusively determine any of these possibilities, if it can be demonstrated that $\Delta\mu_H^+$ affects the intensity of the $\nu_{Fe\text{-}His}$ band, the intensity change could be related to respiratory control, because the Fe−His bond affects the oxygen affinity at its *trans* position.[35]

Helix X is located between hemes a_3 and a, providing the heme axial ligands (His376 and His378 to hemes a_3 and a, respectively).[36] This helix was reported to exhibit a conformational change upon redox and ligation changes of heme a_3, and therefore, it was proposed that it plays a role in gating of H^+ or H_2O molecules in the H pathway.[30,37] Because the axial orientation of helix X is approximately perpendicular to the mitochondrial inner membrane and it has an electric dipole moment along with C═O···HN direction, $\Delta\mu_H^+$ could lead to perturbation of the conformation of helix X, resulting in control of the reaction.[37,38]

The RR spectra recorded for COV at shorter and longer time periods after the full reduction (T_5) under electron-rich and O_2-deficient conditions (spectra A and B of Figure 6, respectively) indicate that CcO approaches the mixed-valence state ($a^{2+}a_3^{3+}$). This was confirmed by the similarity of the spectrum of Figure 6C to the spectrum of Figure 7C, which is the CN^--bound form ($a^{2+}a_3^{3+}$-CN^-). The observation that CcO in COV adopts the $a^{2+}a_3^{3+}$ state in the presence of $\Delta\mu_H^+$ under electron-rich and O_2-deficient conditions appears to be in contrast to the rapid reduction of heme a_3 in the absence of $\Delta\mu_H^+$. This can be seen by comparing the 443 nm solid and broken traces in Figure 3. Because the depth of Fe of hemes a and a_3 in the inner mitochondrial membrane is identical (approximately 1 nm from the positive surface of the membrane), the effects of the electric field by $\Delta\mu_H^+$ on Fe itself are similar. Thus, the structural change that influences the electron transfer rate between hemes a and a_3 might depend upon a particular conformation of the side chains of heme and nearby residues or helix X. No such structural change was clearly detected in this study but might be detectable after application of ultraviolet RR spectroscopy to this COV system. Ultraviolet RR spectroscopy could reveal the vibrational spectra of aromatic amino acid residues preferentially.[39] This technique has been applied to CcO in investigations of the solubilized state.[40] The structural change of tryptophan and tyrosine residues inside or outside of the heme pocket or in the interaction site between cyt c and CcO in the presence of $\Delta\mu_H^+$ can be detected by ultraviolet RR spectroscopy.

■ CONCLUSIONS

A practical method for preparing COV suitable for RR measurements has been developed. The COV has a high RCR value and is tolerant of the laser illumination used for RR measurements. RR spectra reveal that COV placed under electron-rich and O_2-deficient conditions in the presence of

dx.doi.org/10.1021/bi501022j | Biochemistry 2014, 53, 6382−6391

$\Delta\mu_H^+$ adopts the mixed-valence state ($a^{2+}a_3^{3+}$), although it quickly reaches the fully reduced state ($a^{2+}a_3^{2+}$) in the absence of $\Delta\mu_H^+$. The process of reconstituting CcO into COV slightly alters the conformation of the Fe−His bond (heme a_3^{2+}) and the interaction between heme *a* and helix X.

■ ASSOCIATED CONTENT

Supporting Information

Figures S1−S6, measurement of RCR, cell for Raman and absorption measurements, absorption spectra of rhodamine123, response of rhodamine123 in vesicles to a change in pH, pH-dependent absorbance change of rhodamine123, and absorption spectra of cytochrome *c*. This material is available free of charge via the Internet at http://pubs.acs.org.

■ AUTHOR INFORMATION

Corresponding Author

*E-mail: ogura@sci.u-hyogo.ac.jp. Phone: +81-791-58-2938.

Funding

This study was supported by a Grant-in-Aid for Scientific Research on Innovative Areas (Area 2408, No. 25109540) from MEXT, Japan, to T.O.

Notes

The authors declare no competing financial interest.

■ ACKNOWLEDGMENTS

We thank Prof. S. Papa (University of Bali) for the original protocol for preparation of COV and Prof. T. Kitagawa (University of Hyogo) for helpful discussions.

■ ABBREVIATIONS

CcO, cytochrome *c* oxidase; CL, cardiolipin disodium salt; COV, cytochrome *c* oxidase reconstituted in phospholipid vesicles; cyt *c*, cytochrome *c*; $\Delta\mu_H^+$, proton motive force; $\Delta\psi$, electric potential across the membrane; FCCP, carbonyl cyanide-*p*-trifluoromethoxyphenylhydrazone; PC, L-α-phosphatidylcholine; PE, L-α-phosphatidylethanolamine; RCR, respiratory control ratio; Rh, rhodamine123; RR, resonance Raman.

■ REFERENCES

(1) Mitchell, P. (1966) *Chemiosmotic Coupling in Oxidative and Photosynthetic Phosphorylation*, Glynn Research Ltd., Bodmin, U.K., pp 192.

(2) Babcock, G. T., and Wikstrom, M. (1992) Oxygen activation and the conservation of energy in cell respiration. *Nature 356*, 301−309.

(3) Mitchell, P., and Moyle, J. (1969) Estimation of membrane potential and pH difference across the cristae membrane of rat liver mitochondria. *Eur. J. Biochem. 7*, 471−484.

(4) Niemeyer, H., Crane, R. K., Kennedy, E. P., and Lipmann, F. (1951) Observations on respiration and phosphorylation with liver mitochondria of normal, hypo-, and hyperthyroid rats. *Fed. Proc. 10*, 229.

(5) Rabinovitz, M., Stullberg, M. P., and Boyer, P. D. (1951) The Control of Pyruvate Oxidation in a Cell-free Rat Heart Preparation by Phosphate Acceptors. *Science 114*, 641−642.

(6) Lardy, H. A., and Wellman, H. (1952) Oxidative phosphorylations: Role of inorganic phosphate and acceptor systems in control of metabolic rates. *J. Biol. Chem. 195*, 215−224.

(7) Ernster, L., and Luft, R. (1964) Mitochondrial respiratory control: Biochemical, physiological, and pathological aspects. *Adv. Metab. Disord. 1*, 95−123.

(8) Wikstrom, M. (1981) Energy-dependent reversal of the cytochrome oxidase reaction. *Proc. Natl. Acad. Sci. U.S.A. 78*, 4051−4054.

(9) Kadenback, B. (1986) Regulation of respiration and ATP synthesis in higher organisms: Hypothesis. *J. Bioenerg. Biomembr. 18*, 39−54.

(10) Ferguson-Miller, S., and Babcock, G. T. (1996) Heme/Copper Terminal Oxidases. *Chem. Rev. 96*, 2889−2908.

(11) Kitagawa, T., and Ogura, T. (1997) Oxygen activation mechanism at the binuclear site of heme−copper oxidase superfamily as revealed by time-resolved resonance Raman spectroscopy. *Prog. Inorg. Chem. 45*, 431−479.

(12) Han, S., Takahashi, S., and Rousseau, D. L. (2000) Time Dependence of the Catalytic Intermediates in Cytochrome *c* Oxidase. *J. Biol. Chem. 275*, 1910−1919.

(13) Adar, F., and Erecinska, M. (1978) Resonance Raman spectra of whole mitochondria. *Biochemistry 17*, 5485−5488.

(14) Ogura, T. (2012) Resonance Raman applications in investigations of cytochrome *c* oxidase. *Biochim. Biophys. Acta 1817*, 575−578.

(15) Casey, R. P., Chappell, J. B., and Azzi, A. (1979) Limited-turnover studies on proton translocation in reconstituted cytochrome *c* oxidase-containing vesicles. *Biochem. J. 182*, 149−156.

(16) Hinkle, P. C., Kim, J. J., and Racker, E. (1972) Ion Transport and Respiratory Control in Vesicles Formed from Cytochrome Oxidase and Phospholipids. *J. Biol. Chem. 247*, 1338−1339.

(17) Capitanio, N., Capitanio, G., Demarinis, D. A., De Nitto, E., Massari, S., and Papa, S. (1996) Factors Affecting the H^+/e^- Stoichiometry in Mitochondrial Cytochrome *c* Oxidase: Influence of the Rate of Electron Flow and Transmembrane ΔpH. *Biochemistry 35*, 10800−10806.

(18) Sone, N., and Hinkle, P. C. (1982) Proton transport by cytochrome *c* oxidase from the thermophilic bacterium PS3 reconstituted in liposomes. *J. Biol. Chem. 257*, 12600−12604.

(19) Salomonsson, L., Faxen, K., Adelroth, P., and Brzezinski, P. (2005) The timing of proton migration in membrane-reconstituted cytochrome *c* oxidase. *Proc. Natl. Acad. Sci. U.S.A. 102*, 17624−17629.

(20) Paolo, S., Alfredo, C., Maurizio, B. T., Michael, W. T., and Eraldo, A. (1983) Kinetic studies on cytochrome *c* oxidase inserted into liposomal vesicles. Effect of ionophores. *Biochem. J. 209*, 81−89.

(21) Yoshikawa, S., Choc, M. G., O'Toole, M. C., and Caughey, W. S. (1977) An infrared study of CO binding to heart cytochrome c oxidase and hemoglobin A. Implications re O_2 reactions. *J. Biol. Chem. 252*, 5498−5508.

(22) Mochizuki, M., Aoyama, H., Shinzawa-Itoh, K., Usui, T., Tsukihara, T., and Yoshikawa, S. (1999) Quantitative Reevaluation of the Redox Active Sites of Crystalline Bovine Heart Cytochrome *c* Oxidase. *J. Biol. Chem. 274*, 33403−33411.

(23) Baracca, A., Sgarbi, G., Solaini, G., and Lenaz, G. (2003) Rhodamine 123 as a probe of mitochondrial membrane potential: Evaluation of proton flux through F_0 during ATP synthesis. *Biochim. Biophys. Acta 1606*, 137−146.

(24) Ching, Y.-C., Argade, P. V., and Rousseau, D. L. (1985) Resonance Raman spectra of CN^--bound cytochrome oxidase: Spectral isolation of cytochromes a^{2+}, a_3^{2+} and $a_3^{2+}(CN^-)$. *Biochemistry 24*, 4938−4946.

(25) Ogura, T., Hon-nami, K., Oshima, T., Yoshikawa, S., and Kitagawa, T. (1983) Iron-histidine stretching Raman lines of the aa_3-type cytochrome oxidases. *J. Am. Chem. Soc. 105*, 7781−7783.

(26) Li, X.-Y., Czernuszewicz, R. S., Kincaid, J. R., and Spiro, T. G. (1989) Consistent porphyrin force field. 3. Out-of-plane modes in the resonance Raman spectra of planar and ruffled nickel octaethylporphyrin. *J. Am. Chem. Soc. 111*, 7012−7023.

(27) Blackwood, M. E., Jr., Rush, T. S., III, Romesberg, F., Schultz, P. G., and Spiro, T. G. (1998) Alternative Modes of Substrate Distortion in Enzyme and Antibody Catalyzed Ferrochelation Reactions. *Biochemistry 37*, 779−782.

(28) Podstawka, E., Mak, P. J., Kincaid, J. R., and Proniewicz, L. M. (1998) Low frequency resonance Raman spectra of isolated α and β subunits of hemoglobin and their deuterated analogues. *Biopolymers 83*, 455−466.

(29) Takahashi, T., Kuroiwa, S., Ogura, T., and Yoshikawa, S. (2005) Probing the Oxygen Activation Reaction in Intact Whole Mitochondria through Analysis of Molecular Vibrations. *J. Am. Chem. Soc. 127*, 9970−9971.
(30) Muramoto, K., Ohta, K., Shinzawa-Itoh, K., Kanda, K., Taniguchi, M., Nabekura, H., Yamashita, E., Tsukihara, T., and Yoshikawa, S. (2010) Bovine cytochrome *c* oxidase structures enable O_2 reduction with minimization of reactive oxygens and provide a proton-pumping gate. *Proc. Natl. Acad. Sci. U.S.A. 107*, 7740−7745.
(31) Ogura, T., Yoshikawa, S., and Kitagawa, T. (1985) Resonance Raman study on photoreduction of cytochrome *c* oxidase: Distinction of cytochromes *a* and a_3 in the intermediate oxidation states. *Biochemistry 24*, 7746−7752.
(32) Ishigami, I., Nishigaki, T., Shinzawa-Itoh, K., Yoshikawa, S., Nakashima, S., and Ogura, T. (2012) An intermediate conformational state during ligand binding to cytochrome *c* oxidase detected by time-resolved resonance Raman analyses of heme peripheral groups. *Chem. Lett. 41*, 178−180.
(33) Bangcharoenpaurpong, O., Schomacker, K. T., and Champion, P. M. (1984) A Resonance Raman Investigation of Myoglobin and Hemoglobin. *J. Am. Chem. Soc. 106*, 5688−5698.
(34) Stavrov, S. S. (1993) The Effect of Iron Displacement Out of the Porphyrin Plane on the Resonance Raman Spectra of Heme Proteins and Iron Porphyrins. *Biophys. J. 65*, 1942−1950.
(35) Matsukawa, S., Mawatari, K., Yoneyama, Y., and Kitagawa, T. (1985) Correlation between the iron-histidine stretching frequencies and oxygen affinity of hemoglobins. A continuous strain model. *J. Am. Chem. Soc. 107*, 1108−1113.
(36) Tsukihara, T., Aoyama, H., Yamashita, E., Tomizaki, T., Yamaguchi, H., Shinzawa-Itoh, K., Nakashima, R., Yaono, R., and Yoshikawa, S. (1995) Structures of metal sites of oxidized bovine heart cytochrome *c* oxidase at 2.8 Å. *Science 269*, 1069−1074.
(37) Nakashima, S., Ogura, T., and Kitagawa, T. (2014) Infrared and Raman spectroscopic studies on the reaction mechanism of cytochorome *c* oxidase. *Biochim. Biophys. Acta*, DOI: 10.1016/j.bbabio.2014.08.002.
(38) Kubo, M., Nakashima, S., Yamaguchi, S., Ogura, T., Mochizuki, M., Kang, J., Tateno, M., Shinzawa-Itoh, K., and Yoshikawa, S. (2013) Effective Pumping Proton Collection Facilitated by a Copper Site (Cu_B) of Bovine Heart Cytochrome *c* Oxidase, Revealed by a Newly Developed Time-resolved Infrared System. *J. Biol. Chem. 288*, 30259−30269.
(39) Asher, S. A., Ludwig, M., and Johnson, C. R. (1986) UV resonance Raman excitation profiles of the aromatic amino acids. *J. Am. Chem. Soc. 108*, 3186−3197.
(40) Aki, M., Ogura, T., Naruta, Y., Le, T. H., Sato, T., and Kitagawa, T. (2002) UV resonance Raman characterization of model compounds of Tyr244 of bovine cytochrome *c* oxidase in its neutral, deprotonated anionic, and deprotonated neutral radical forms: Effects of covalent binding between tyrosine and histidine. *J. Phys. Chem. A 106*, 3436−3444.